A Full-Scale Particle Image Velocimetry Investigation of "Young" Rotor Blade Tip Vortices

K. Kindler[1], K. Mulleners[1]*, H. Richard[1], and M. Raffel[1]

[1]Institute for Aerodynamics and Flow Technology,
German Aerospace Centre, Göttingen,
Bunsenstrasse 10, D-37073 Göttingen, Germany,
*E-mail: Karen.Mulleners@dlr.de

Abstract

The blade tip vortex of a full-scale MBB Bo 105 Helicopter is investigated experimentally under simulated hover flight conditions in ground effect by means of stereoscopic Particle Image Velocimetry. Based on the three-component velocity field of azimuthal vortex ages of $\psi = 1°$, $3°$, $5°$, $10°$, $20°$ and $30°$ vortex core radii, peak velocities, and vorticities are quantified and compared to model-scale experimental results available in literature and Vatistas' low-order model for concentrated vortices. The vortex velocity profiles are found to be in satisfactory agreement with the model whereas the experimentally limited spatial resolution of the velocity fields results in a slight overestimation of the core radii and an underestimation of peak velocities as compared to model-scale investigations. Finally, an attempt has been made to cross-validate full-scale blade tip vortex parameters derived from Background Oriented Schlieren measurements using natural formation backgrounds.

Introduction

The blade tip vortices shed from the main rotor of a helicopter might be considered the dominant coherent structures of the rotor wake, especially, with a view to fluid–structure interaction, aeroacoustics, etc. As such the blade tip vortex has drawn considerable attention in terms of analytical, experimental, and increasingly numerical investigations during the past decades [1].

Due to the inherent complexity of the helicopter flow field, experimental as well as numerical investigations are usually rather intricate, time-consuming, and, cost-intensive. Therefore, it is appealing to think about the adaptation of available experimental methods capable of probing the blade tip vortex characteristics of full-scale helicopters *in situ*, i.e. in flight. Obviously, such full-scale experiments could provide validation data for numerical simulations or model predictions for a larger range of flight attitudes than typically accessible in wind tunnel testing and issues of e.g. blade–vortex or structure–vortex interactions could be directly addressed even during prototyping. It should be noted that both design and flight parameters are equally interesting to consider as the strength of the tip vortex strongly depends on thrust and the blade tip geometry [2].

There are at least two methods at hand which have already been integrated and employed for ground independent full-scale measurements. Those are Light Detection and Ranging (LIDAR) based on portable fibre lasers measuring local velocities, and Background Oriented Schlieren (BOS) imaging density gradients within the flow field. The former requires the scanning of tip vortex cross-sections while the latter has recently been employed to derive core density estimations of "young" blade

Presented at the American Helicopter Society 65th Annual Forum, Grapevine, Texas, May 27-29, 2009.

tip vortices ($\psi \leq 3^\circ$) in hover conditions in ground effect [4]. The core radius and core density depression in this study have been found to be consistent with the Scully vortex.

However, in order to experimentally verify the validity of a particular vortex model or the vortex parameters determined, the velocity field of the blade tip vortex has to be quantified. In continuation of the feasibility study by Raffel et al. [9] we report on three-component velocity measurements by means of stereoscopic Particle Image Velocimetry (PIV) at vortex ages ranging from $\psi = 1^\circ$ to 30° in azimuth.
The simple rectangular rotor blade geometry of the test helicopter allows for a comparison with a variety of available experimental model-scale data (see [10] and references therein).

The paper is organised as follows. In the next section the experimental details will be specified along with the data evaluation methodology. The discussion of the results will comprise the derivation of the vortex parameters and a comparative view on recent laboratory and full-scale BOS results followed by the conclusions and some possible future directions.

Experimental Methods

For this study DLR's MBB Bo 105 experimental helicopter was lashed to the ground and operated in simulated hover flight in ground effect. The fixation of the helicopter is experimentally most favourable and the development of tip vortices within the range of azimuth relevant to this study can be anticipated to be well defined. The experimental conditions are similar to those previously employed for first full-scale monoscopic PIV measurements of blade tip vortices [9] and full-scale BOS measurements [4].

Measurement Configuration

The main rotor of the test helicopter has four hinge-less, rectangular plane form blades with a radius of $R = 4.91\,\mathrm{m}$, a chord length of $c = 0.27\,\mathrm{m}$. The angular velocity of the main rotor was $\Omega = 14\pi\,\mathrm{s}^{-1}$ yielding a blade tip Mach number of $Ma = 0.64$. During simulated hover flight, the helicopter generated approximately $T = 20000\,\mathrm{N}$ thrust and the thrust coefficient solidity ratio is estimated as $C_T/\sigma \simeq 0.07$ at ca. -8° blade twist.

The measurement plane was located on the port-side, parallel to the trailing edge of the blade (cf. figure 1). The PIV acquisition system consisted of two $10.5\,\mathrm{Mpx}$ CCD cameras equipped with $f = 300\,\mathrm{mm}$ objectives in a stereoscopic configuration. The cameras were positioned on a vertical support ca. $1.5\,\mathrm{m}$ above and $2.1\,\mathrm{m}$ below the rotor plane in idle condition at a distance of $10\,\mathrm{m}$ off the blade tip. Illumination of the flow field was provided by means of a laser light sheet fed by a double cavity Nd:Yag pulse laser with a wave length of $\lambda = 532\,\mathrm{nm}$ and an energy of $E = 280\,\mathrm{mJ}$ per pulse. The spatial resolution of the image acquisition system was $4\,\mathrm{px/mm}$ for a field of view as large as $1 \times 1.2\,\mathrm{m}^2$. The PIV system was synchronised with the main rotor taking advantage of an inductive rotor position indicator permanently installed for rotor balancing purpose.

With a view to off-laboratory PIV applications, the provision of a homogeneous and sufficiently dense tracer particle distribution is a demanding task. Especially the atmospheric back-

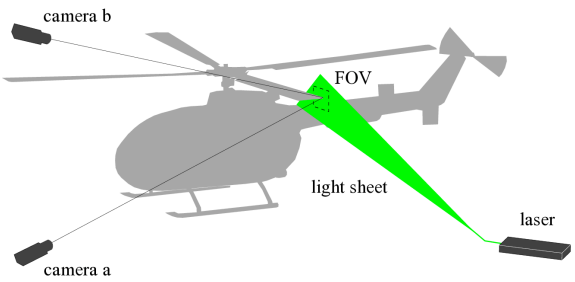

Figure 1: Experimental set-up of the MBB Bo 105 test helicopter for stereoscopic PIV measurements in simulated hover flight in ground effect.

ground conditions, i.e. even moderate cross-winds, might strongly alter the optimal injection point and, therefore, the tracer density within the field of view. Hence, the tracer generation and supply including an injection nozzle reaching approximately 3 m above the rotor disk, were chosen to be realised on a mobile platform which could be relocated in response to the outer conditions at a distance of one rotor radius apart from the rotor disk.

Evaluation Methodology

The stereoscopic PIV data is evaluated according to standard procedures [7]. The intensity images acquired were high-pass filtered and normalised using the series minimum image prior to further processing. A camera view misalignment correction was computed for each time series as part of the image de-warping to compensate for small image offsets which would be greatly amplified due to the large scale geometry of the set-up [6].

Optimising the interrogation window size and overlap the scheme of *Richard & van der Wall* [8] was followed. The interrogation window size was minimised with respect to acceptable signal-to-noise ratios while the window overlap was maximised, to avoid artificial smoothing of steep velocity gradients. In this case yielding $32^2 px$ windows with an overlap of approximately 94%. Additionally, a multi-grid evaluation scheme is used within the correlation analysis, further increasing the resolution of regions of strong shear.

However, the data quality of the full-scale PIV measurements was found to strongly vary for subsequent time steps. The measurement noise level was considerably larger than those typically observed in laboratory experiments. Obviously, these variations are primarily due to varying or intermittently inhomogeneous tracer concentrations within the region of interest. Velocity fields without any or with an apparently strongly dysmorph vortex structure were discarded, corresponding to ca. 10% of a time series of 120 image pairs acquired at each azimuthal position.

Prior to any further analysis the averaged background velocities were subtracted from the instantaneous velocity fields. Subsequently, the vortex centres were identified using the scalar function introduced by *Graftieaux* et al. [3]

$$\Gamma(P) = \frac{1}{S} \int_{M \in S} \frac{(PM \wedge U_M)\hat{e}_z}{\| PM \| \cdot \| U_M \|} dS \qquad (1)$$

where S is the two dimensional neighbourhood of any point P in the x, y plane, M lies in S, $\hat{e}_z$ is the unit vector in z, and the maximum of Γ is identified with the vortex centre. Note that Gamma is not to be confused with the vorticity. Unlike alternative criteria for vortex centre identification such as vorticity peak detection or the like, the Γ function does not require velocity field derivatives or the out of plain component reconstructed during evaluation and, therefore, it is less susceptible to experimental noise.

The inclination of the vortex axis with respect to x and z spanning the measurement plane was found to be smaller than 3.5° for the data relevant to this study which was considered negligible rendering a transformation in the vortex system unnecessary [10].

Results and Discussion

Figure 2 depicts the conditionally averaged velocity and vorticity field of the blade tip vortex at $\psi = 5^\circ$[1] wherein the velocity is scaled by the

[1] The term conditional average denotes alignment of the instantaneous velocity fields with respect to the vortex centre location prior to averaging and is not to be confused with axial averaging.

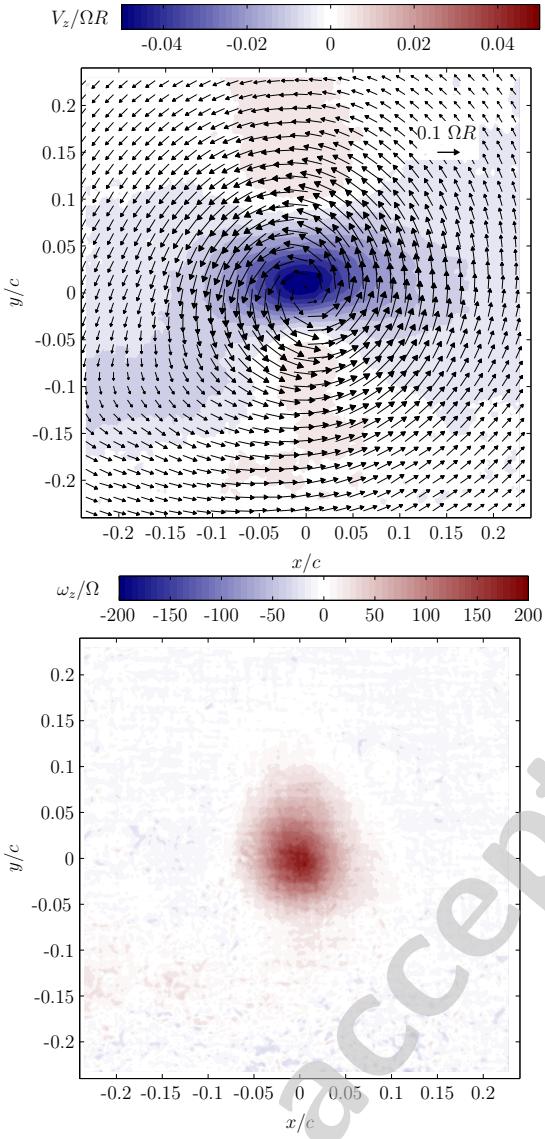

Figure 2: A representative conditionally averaged velocity field (top) and the corresponding in-plane vorticity component (bottom) at $\psi = 5°$.

blade tip speed ΩR while the in-plane component of the vorticity ω_z is scaled by the angular velocity of the main rotor Ω. Consistent with the resulting velocity fields for the other azimuthal ages recorded (not shown here), the in-plane

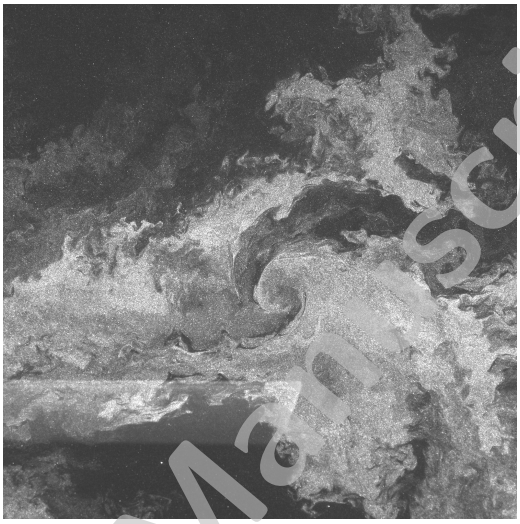

Figure 3: An example of the tracer density and distribution within the region of interest.

velocity field indicates a clean spherical vortex cross-section while the z-component, i.e. the out-of-plane component, exhibits a noticeable dilatation. It is understood that this is an effect of a virtually unavoidable tracer density gradients within the region of interest. In figure 3 an example of the tracer distribution within the raw image is depicted in order to illustrate the particular challenges of full-scale PIV applications. Due to the unsteady nature of the flow field dissociated tracer patches of variable size are most commonly found. Furthermore, injecting tracers from above the rotor plane, the down wash tends to induce higher tracer concentrations inboards the blade tip while the fluid from the recirculation region outboards features stronger "patchiness" and on average lower tracer concentration.

The local tracer density can be thought of as the intrinsic limit of measurement resolution as it defines the minimal interrogation window size, i.e. the probe volume of the PIV. At the same time the correlation analysis of the interrogation windows represents a low pass filter

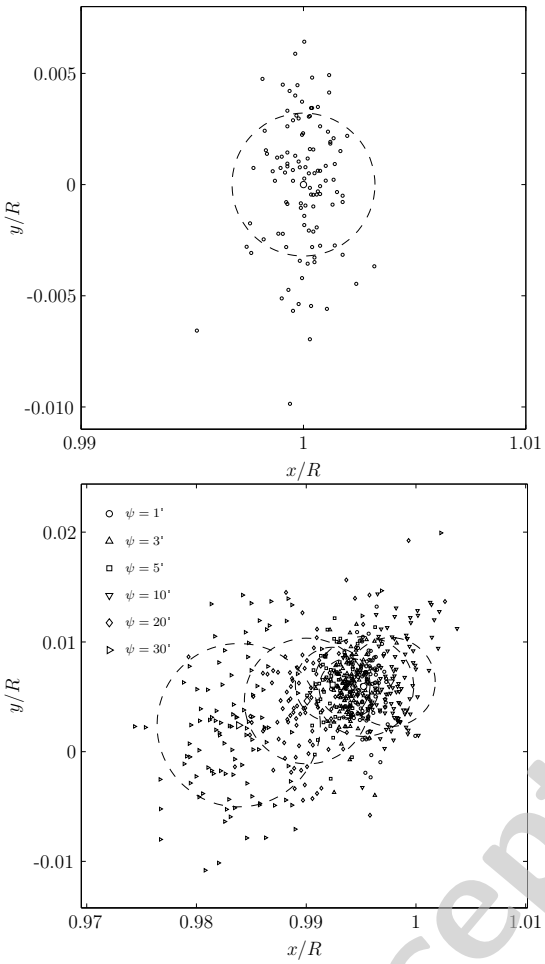

Figure 4: The blade tip (top) and vortex centre position for the different azimuth measured (bottom); larger symbols indicate series mean values while the dashed circles depicted the standard deviation.

limiting the peak velocities accessible [8]. As a measure of physical resolution, the ratio of measurement volume to chord length in this case is $L_m/c=0.0296$ which translates to $L_m/r_c=0.593$ using $r_c=0.05c$ as an estimate of the vortex core radius. We note that this value is close to recent model-scale investigations [10] but, however, at least factor of 3 coarser than the commonly accepted resolution requirement of $L_m/r_c<0.2$ [5].

With regard to the distribution of vortex positions figure 4, it can be seen that the blade tip position itself (top of figure 4) scatters in the range of $\delta y=\pm 0.007R$, i.e. a variation of the flapping angle of $\delta\alpha_{max}=\pm 0.5^\circ$ with a standard deviation of $\delta\alpha=\pm 0.2^\circ$. The distribution of vortex positions at $\psi=1^\circ$ is analogous to the blade tip behaviour and the standard deviation even decreases mildly for $\psi=3^\circ$ and 5°. In consistence with the findings for recent model-scale investigations of comparable rotor geometry and solidity [8] the scattering increases for larger azimuth where the horizontal distribution in the full-scale case appears to be broadened without constraining the comparability for $\psi\leq 30^\circ$.

Vortex Characterisation

Analysing the velocity fields *Vatistas'* vortex model [11] is considered which is reproduced below for convenience. The normalised tangential, radial, and axial velocity take the form

$$\overline{V}_\Theta = \frac{\bar{r}}{(1+\bar{r}^{2n})^{1/n}} \quad , \tag{2}$$

$$\overline{V}_r = -\frac{2(1-n)\bar{r}^{2n-1}}{1+\bar{r}^{2n}} \quad , \tag{3}$$

and

$$\overline{V}_z = \frac{4n(1+n)\bar{r}^{2(n-1)}}{(1+\bar{r}^{2n})^2} \quad , \tag{4}$$

where $\overline{V}_\Theta=V_\Theta/V_{\Theta,0}$ with $V_{\Theta,0}=\Gamma_\infty/2\pi r_c$, $\bar{r}=r/r_c$, $\overline{V}_r=V_r r_c/\nu$, $\overline{V}_z=V_z r_c/\nu$, and $\bar{z}=z/r_c$. Γ_∞ is the circulation, ν is the dynamic viscosity and the core radius r_c and $V_{\Theta,0}$ were determined by least-square fitting. Initially, treating n as fit parameter, values very close to $n=1$ are found for which reason the Scully vortex model was applied in the remainder of the evaluation reducing the degree of freedom of the fit.

In figure 5 the fitted velocity profiles of the conditionally averaged data fields are shown. For these, the tangential, radial, and axial velocity profiles have been averaged

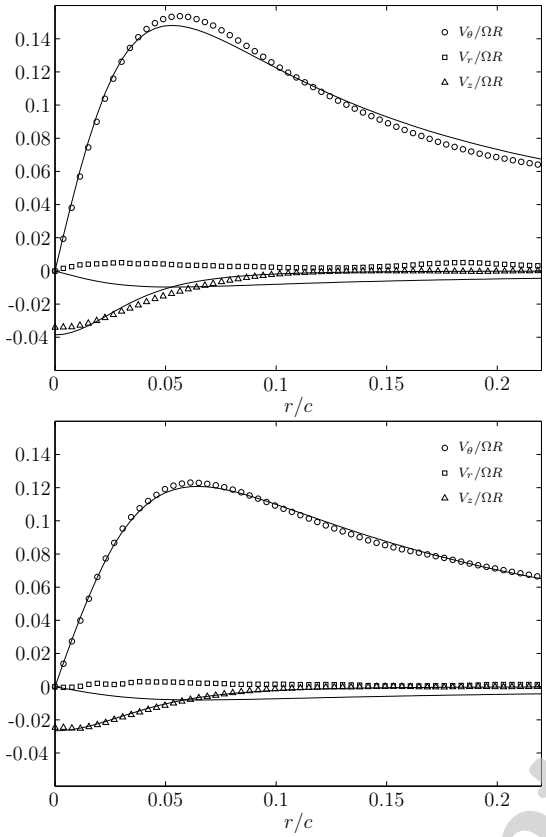

Figure 5: Three-component velocity field of the blade tip vortex at $\psi = 3°$ (top) and $\psi = 30°$ (bottom); lines represent the best fit to equation 2, 3, and 4 using $n = 1$.

with respect to the vortex axis prior to conditionally averaging the time series which then were fitted with the model. Of course, this approach implies axial symmetry of the vortex itself a priori.

Most prominently, the tangential and axial velocity components are consistent with the model of equation 2, and 4 while the radial component exceeds the predicted slope. The relatively weak radial velocity component is particularly sensitive to effects of lateral vortex convection and lacking cross-sectional symmetry. The former is determined from the background, therefore, it is reasonable to associate the poor performance of the radial component partly with the tracer inhomogeneity. Additionally, as is generally known, the down wash depresses the radial velocities inboard of the tip which translates into the velocity profiles by the axial averaging applied.

Comparative Analysis

As the most convenient parameters for a comparison to the model-scale investigations available, the average and time series extrema of the core radii and tangential velocity are summarised in table 1 and 2. The results are consistent with the findings of *van der Wall & Richard* [10, 9] for a Mach-scaled model of the MBB BO 105 main rotor in hover condition with regard to the order of magnitude. Nevertheless, the average core radii in this study are by a factor of approximately 1.5 smaller and the maximum tangential velocities are by a factor of 3 larger than the values reported here. It should be noted that the measurement resolution of the above mentioned study ranges from $L_m/c = 0.51$ to as high as $L_m/c = 0.0124$ which is accountable for the differences in r_c and V_Θ.

The particular method of averaging appears to have only little effect while time series extrema indicate rather large differences of individual velocity fields. Clearly, the majority of the velocity fields is incompletely symmetric. Although based on on a limited sample size of ca. a hundred evaluated fields per azimuth, the distribution of the core radii (cf. figure 6) exhibits a noticeable tale towards larger r_c. The confluence of the various uncertainties in the PIV evaluation

$\psi[°]$	$\overline{r_c}/c$	r_c/c	$r_{c,max}/c$	$r_{c,min}/c$
1	0.070(11)	0.055(11)	0.094	0.039
3	0.055(11)	0.057(11)	0.096	0.036
5	0.059(15)	0.063(15)	0.106	0.041
10	0.059(11)	0.060(11)	0.102	0.042
20	0.067(15)	0.069(15)	0.127	0.043
30	0.066(14)	0.067(14)	0.120	0.042

Table 1: The conditional average $\overline{r_c}/c$ and average instantaneous core radius r_c/c and minimal and maximal series values.

$\psi[^\circ]$	$\overline{V}_\Theta/\Omega R$	$V_\Theta/\Omega R$	$V_{\Theta,max}/\Omega R$	$V_{\Theta,min}/\Omega R$
1	0.138	0.130	0.205	0.067
3	0.149	0.148	0.231	0.051
5	0.145	0.142	0.215	0.069
10	0.145	0.142	0.223	0.084
20	0.128	0.125	0.182	0.063
30	0.123	0.121	0.192	0.070

Table 2: The conditional average $\overline{V}_\Theta/\Omega R$ and average instantaneous peak tangential velocity $V_\Theta/\Omega R$ and minimal and maximal series values.

attenuates the velocity gradients tending to overestimate r_c.

In the range of azimuthal age considered here from both the maximal tangential velocity and the core radii at this point no consistent trend is observed, i.e. effects of vortex ageing are below the measurement noise level. However, provided averaging effects can be reduced by an extended post-processing which is currently being implemented effects of vortex ageing will be dissected.

Comparing the averaged instantaneous vortex radii determined from three-component velocity measurements with the corresponding values derived from BOS measurements, $r_c/c = 0.049$ and 0.060 for $\psi = 1^\circ$ and 3° respectively, the deviations are negligibly small (0.002 and $0.007/c$). Not surprisingly, the BOS results compare best with the averaged core radii as Schlieren are an integral measurement technique and, secondly, the reconstruction algorithm used in [4] implicitly assumes axial symmetry.

Despite the uncertainties mentioned above the BOS results are sufficiently validated to proceed to studying blade tip vortices under further flight conditions. Furthermore, a refinement of the PIV evaluation scheme is continuously being worked on which can be expected to further improve the vortex parameter results.

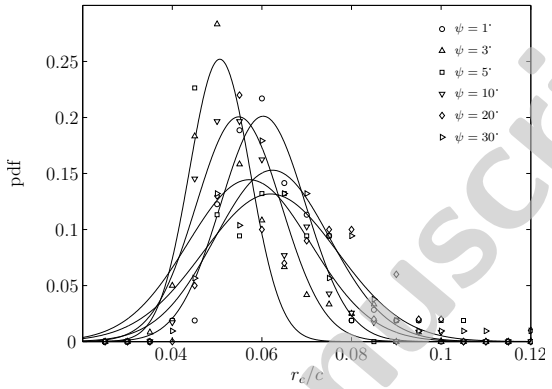

Figure 6: The probability density of the core radii for the different vortex ages. The Gaussian distributions are intended to illustrate the width of the distribution, serving as a guide to the eye.

Comments on Full-Scale PIV Testing

As we noticed an increasing interest in full scale, off-laboratory, non-intrusive velocity measurements both from the scientific as well as, at least partly, from the industrial community a few considerations shall be added here.

As pointed out above, the tracer density defining the signal to noise ratio and the resolution of the velocity field is clearly the limiting factor in terms of the data quality. More precisely, the homogeneity of the measurement volume tracer density distribution is the crucial parameter for which reason we believe that measurement techniques accepting lower absolute tracer densities than PIV such as Laser Doppler Anemometry (LDA) or LIDAR are equally effected. As fluid entrainment, environmental effects, and turbulence generate a constant large scale fluid exchange one can think about employing atmospheric aerosols or particles in order to avoid artificial tracer injection and distribution issues. However, the corresponding atmospheric conditions remain to be defined and true in-flight PIV applications are rather intricate to implement.

Therefore, we chose to concentrate on the integration of an airborne BOS system which is

much less demanding concerning its technical as well as legal, i.e. certification, aspects. In conclusion, to date, regarding viscous vortical structures BOS appears the more efficient approach.

Conclusions

Three component velocity fields of the blade tip vortices of a full-scale BO 105 helicopter have been presented and discussed in relation to Vatistas' vortex model. The vortex parameters derived from the PIV measurements are found to be consistent with recent model-scale investigations and, coincidentally, these results confirm earlier full-scale BOS measurements of "young" blade tip vortices. Further pursuing this approach an airborne, rotor synchronised image acquisition system is currently being developed and certified which will be utilised to study tip vortex characteristics *in situ* under various flight conditions.

Acknowledgements

This work has been part of the European Commission funded project "Advanced In-Flight Measurement Techniques" (AIM) and the analysis has partly been performed in the framework of the US/German Memorandum of Understanding on Helicopter Aerodynamics, Task VIII "Rotor Wake Measurement Techniques". Furthermore, the dedicated support by R Gebhard and U. Göhmann from DLR's flight facilities in Braunschweig as well as by our colleagues M. Jönsson and M. Kühn is gratefully acknowledged.

References

[1] A.T. Conlisk. Modern helicopter aerodynamics. *Ann. Rev. Fluid Mech.*, 29:515, 1997.

[2] A.T. Conlisk. Modern helicopter rotor aerodynamics. *Progr. in Aerospace Sci.*, 37:419, 2001.

[3] L. Graftieaux, M. Michard, and N. Grosjean. Combining piv, pod and vortex identification algorithms for the study of unsteady turbulent swirling flows. *Meas. Sci. Technol.*, 12:1422, 2001.

[4] K. Kindler, E. Goldhahn, F. Leopold, and M. Raffel. Recent developments in background oriented schlieren methods for rotor blade tip vortex measurements. *Exp. Fluids*, 43:233, 2007.

[5] P.B. Martin, J.G. Pugliese, J.G. Leishman, and S.L. Anderson. Stereo PIV measurements in the wake of a hovering rotor. In *56th Ann. Forum of the American Helicopter Society, Virginia Beach, USA, May 2–4*, 2000.

[6] M. Raffel, U. Seelhorst, and C. Willert. Recording and evaluation methods of PIV investigations on a helicopter rotor model. *Exp. Fluids*, 36:146, 2004.

[7] M. Raffel, C. Willert, S. Wereley, and J. Kompenhans. *Particle Image Velocimetry, A practical guide*. Springer, 2004.

[8] H. Richard, J. Bosbach, A. Henning, M. Raffel, and B. van der Wall. 2c and 3c piv measurements on a rotor in hover condition. In *13th Int. Symp. on Applications of Laser Techniques to Fluid Mechanics, Lisbon, Portugal, June 26–29*, 2006.

[9] H. Richard and M. Raffel. Rotor wake measurements: Full-scale and model tests. In *AHS 58th Ann. Forum, Montréal, Canada, June 11–13*, 2002.

[10] B. van der Wall and H. Richard. Analysis methodology for 3c-piv data of rotary wing vortices. *Exp. Fluids*, 40:798, 2006.

[11] G.H. Vatistas, V. Kozel, and W.C. Mih. A simpler model for concentrated vortices. *Exp. Fluids*, 11:73, 1991.